ISPRS Journal of Photogrammetry and Remote Sensing 66 (2011) 498–507

Contents lists available at ScienceDirect

ISPRS Journal of Photogrammetry and Remote Sensing

journal homepage: www.elsevier.com/locate/isprsjprs

Angular effect of MODIS emissivity products and its application to the split-window algorithm☆

Huazhong Ren [a], Guangjian Yan [a,*], Ling Chen [a], Zhaoliang Li [a,b]

[a] State Key Laboratory of Remote Sensing Science, School of Geography, Beijing Normal University, Beijing 100875, China
[b] Institute of Geographic Science and Natural Resources Research, Chinese Academy of Science, Beijing 100101, China

ARTICLE INFO

Article history:
Received 14 January 2010
Received in revised form
29 October 2010
Accepted 13 February 2011
Available online 15 March 2011

Keywords:
MODIS emissivity
Angular effects
Split-window algorithm

ABSTRACT

The angular effects of emissivity are ignored in current land surface temperature (LST) products. As a result, the directionality of these LST products limits their further application in many fields. Accurate correction of the angular problem of LST products requires explicit understanding of the angular effects of emissivity at the pixel scale. Currently, nearly ten years of global emissivity products of MODIS are available. However, the pixel-scale directionality of emissivity has never been analyzed. By performing a statistical analysis of 5-year MODIS emissivity products over most of East Asia, we generated the empirical relationships between the directional emissivity, land cover, and seasonal variations. Two look-up tables (LUTs) of directional emissivity were created for typical land cover types and applied to the generalized *split-window algorithm* to modify the MODIS LST. The results showed that the angular effect of emissivity could introduce a significant bias of −1–3 K to the 1 km resolution LST. Finally, the spatial scale effects of emissivity were analyzed, and it was found that the temperature differences caused by scale effects fell within +/−0.5 K for most pixels if 5 km emissivity was used in 1 km LST retrieval. Therefore, wide use of the LUTs can be expected.

1. Introduction

Land surface temperature (LST) is one of the key parameters in land surface processes, and it has been widely used in studying regional energy budgets, climatic changes, and watershed management and crop assessments (Mannstein, 1987; Su, 2002). The development of satellite and sensor technology in recent decades has provided us with an opportunity to retrieve the LST from remotely sensed data (Kahle et al., 1980). Several approaches have been proposed to retrieve the LST, such as the *single-channel* method (Duan et al., 2008; Jiménez-Muñoz and Sobrino, 2003; Price, 1983; Qin et al., 2001) and the *split-window algorithm* (Becker and Li, 1990b; McMillin, 1975; Wan and Dozier, 1996). However, the inversion of the LST is always an underdetermined problem because there are more unknowns than measurements even when the atmospheric temperature and humidity profiles are exactly known. Such an ill-posed problem makes the retrieving process difficult (Wan and Li, 1997). Emissivity plays a crucial role in the inversion of the LST, and its error affects the accuracy of the LST; for example, an uncertainty on the emissivity of 0.01 can lead to an error on the LST of around 0.5 K (Sobrino et al., 2005).

For LST retrieval using remotely sensed data, pixel-scale emissivity is required instead of the in situ measurement at several fixed points. Many methods have been developed to obtain pixel emissivities. Some of them used thermal spectral indices, such as the TISI (Becker and Li, 1990a), ISSTES (Borel, 1998; Ingram and Muse, 2001) and the alpha residuals methods (Kealy and Hook, 1993; Watson, 1992). Van and Owe (1993) and Enric and Vicente (1996) proposed an empirical method to obtain the emissivity from the normalized difference vegetation index (NDVI); Gillespie et al. (1998) developed a temperature and emissivity separation (TES) algorithm to retrieve the emissivity from five thermal bands of ASTER, and the accuracy of emissivity can reach 0.015 in clear-sky conditions.

The emissivities of natural objects are affected by the viewing angles (Zhao, 2003). The angular dependence of emissivity has been studied by using field and laboratory measurements (Barton and Talashima, 1986; Chen et al., 2000; Petitcolin et al., 2002a,b; Kimes and Kirchener, 1983; Labed and Stoll, 1991; Lagouarde et al., 1995; Su et al., 2000a). Their results indicated that the emissivities of bare soil, sand, clay, and water decreased with

☆ The work has been partially supported by the NSFC (Grant no. 40871164), National Basic Research Program of China, 973 Program (Grant no. 2007CB714402), and the European Commission (Call FP7-ENV-2007-1 Grant no. 212921) as part of the CEOP-AEGIS project (http://www.ceop-aegis.org/) coordinated by the Université de Strasbourg.

* Corresponding author. Tel.: +86 10 58802085.
E-mail address: gjyan@bnu.edu.cn (G. Yan).

0924-2716/$ – see front matter © 2011 International Society for Photogrammetry and Remote Sensing, Inc. (ISPRS). Published by Elsevier B.V. All rights reserved.
doi:10.1016/j.isprsjprs.2011.02.008

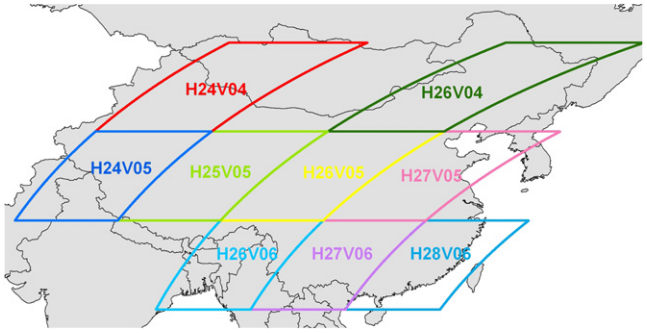

Fig. 1. The study region, located in East Asia, from 19°59′ N to 49°59′ N latitude and from 69°17′ E to 155°59′ E longitude, including most of China, Mongolia, and Russia.

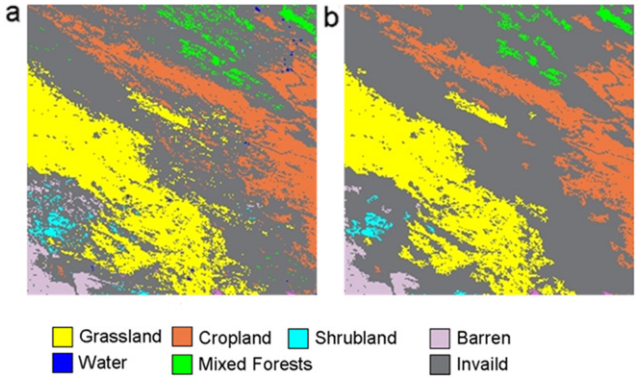

Fig. 3. A comparison between the images before and after cluster analysis on MODIS tile H26V04 in 2001.

increasing viewing angle, but for dense vegetated canopies the angular dependence is minimal (Sobrino et al., 2005). Other studies have addressed modeling the angular variation of emissivity. Prata (1993) proposed a simple way to obtain the directional emissivity as $\varepsilon(\theta) = \varepsilon(0)\cos(\theta/2)$, where θ is the viewing angle and $\varepsilon(0)$ is the nadir emissivity. Such an equation is simple but is not applicable for all land cover types due to heterogeneity. Sobrino et al. (2005) classified these methodologies into two categories: geometrical models (GMs) and radiative transfer (RT) models. A GM estimates the thermal infrared (TIR) radiance at the sensor level by combining the weight of proportions and thermal radiance from several components. For example, Sobrino and Caselles (1990) applied a GM to describe the directional emissivity of row-distributed crops, and this model was later extended by Caselles and Sobrino (1992). Moreover, Snyder et al. (1998) extended the geometric–optical BRDF model for a sparse forestry field (Li and Strahler, 1992) to the TIR region with a linear kernel approximation and calculated the "classification-based emissivity" of several land cover types. Such classification-based emissivities were used to recover the MODIS LST (Wan and Dozier, 1996). Geometrical models treat the vegetation as solids and thus cannot realistically represent multiple scattering within the canopy. In contrast, RT models simulate the TIR radiation propagation and interactions within the canopy and the atmosphere. For example, François et al. (1997) proposed an analytical parameterization model for emissivity based on the gap function. Verhoef et al. (2007) and Liu et al. (2003) introduced an additional radiative resource to the SAIL (scattering by arbitrarily inclined leaves) model to extend its application to the thermal infrared domain. Li et al. (1999) took into account the component temperature differences in a non-isothermal pixel, and proposed the concept of "apparent emissivity increment". Such a model, named the LSF model, was expected to describe the effective directional emissivity for non-isothermal surfaces and was validated by several field measurements and computational simulation (Su et al., 2000b,c), but its application to remote sensing data is limited due to the lack of an objective reference temperature.

The angular variation of pixel-level emissivity is hard to know due to the lack of multi-angle space-borne thermal sensors and effective emissivity retrieval algorithms; this has really reduced the accuracy of the LST and its application. Up to now, nearly ten years of global MODIS emissivity products from the *day/night algorithm* are available but they have never been

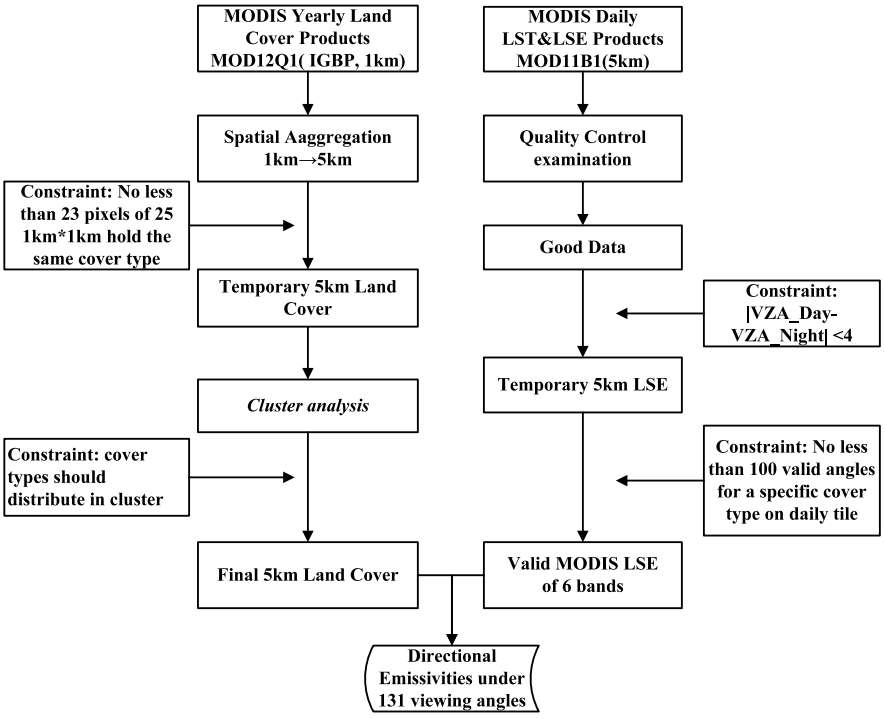

Fig. 2. The data-picking flowchart to retrieve the directional emissivity.

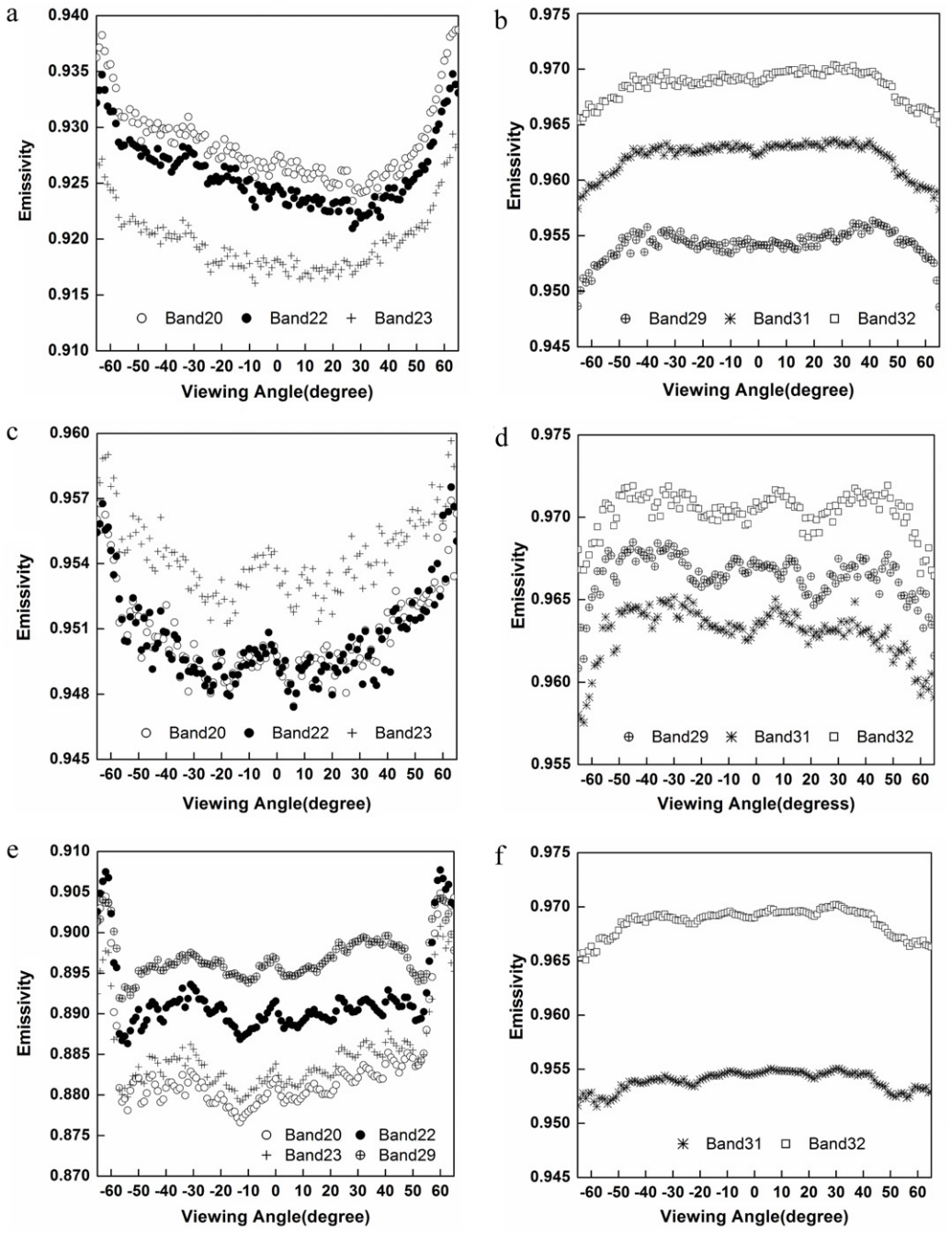

Fig. 4. Directional emissivities in MODIS MIR and TIR bands. (a) (b), for *Grassland* in the MIR and TIR bands, (c), (d) for *Cropland*; (e), (f) for *Barren*. The band 29 emissivity for *Barren* varied similarly to those in the MIR bands shown in (e).

used to obtain the directional emissivity. We analyzed the angular variation of emissivity at the pixel scale using MODIS LST and emissivity (LST&LSE) products from the *day/night algorithm*, and applied such knowledge to the *split-window algorithm* for angular correction of the LST. The next section gives a brief description of MODIS LST&LSE products and the methods used to obtain the characteristics of the directional emissivity. Section 3 presents the angular variation and seasonal variation of emissivities. Section 4 shows the angular correction results that were obtained using the newly created look-up table of directional emissivity, and compares them with the original MODIS LST products. Section 5 is an attempt to understand the spatial scale effect between 1 and 5 km LST values if the 5 km emissivity is used in the *split-window algorithm*.

2. Materials and methods

2.1. MODIS LST&LSE products and land cover products

By using middle and thermal infrared (MIR&TIR) measurements, MODIS land surface products can provide global daily or quasi-daily LST&LSE including the 1 km spatial resolution LST generated by the generalized *split-window algorithm* (Wan and Dozier, 1996) or the 5 km/6 km value estimated by the *day/night algorithm* (Wan and Li, 1997). The physically based *day/night algorithm* retrieves the surface spectral emissivity and LST from a pair of daytime and nighttime MODIS data in MIR bands (20: 3.66–3.84 μm, 22: 3.929–3.9894 μm, 23: 4.02–4.08 μm) and TIR bands (29: 8.4–8.7 μm, 31: 10.78–11.28 μm, 32: 1.77–12.27 μm). Considering the angular variation in emissivity, this algorithm

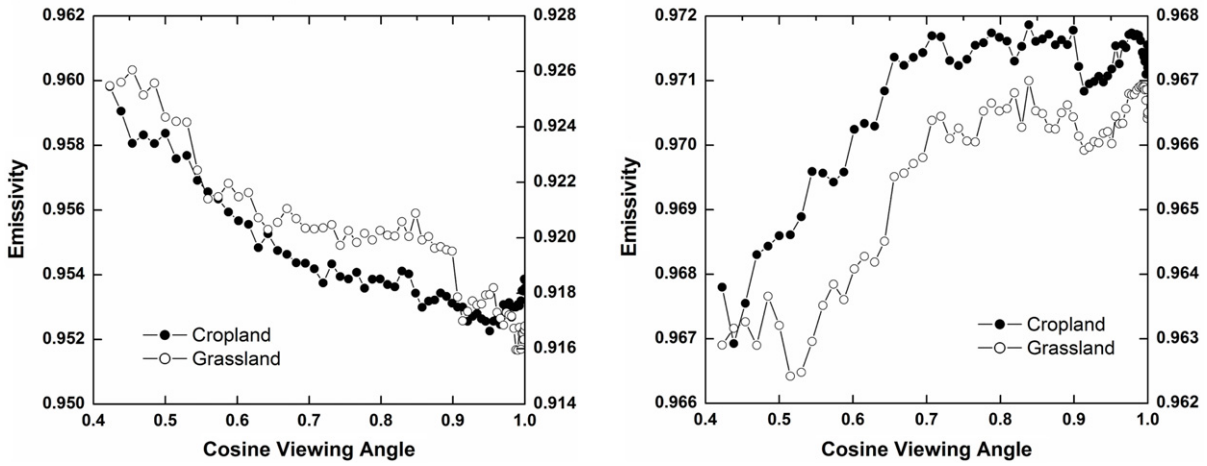

(a) Band 23. (b) Band 32.

Fig. 5. Directional emissivity versus the cosine of the viewing angle for *Cropland* and *Grassland* in band 23 (a) and band 32 (b) of MODIS. The right *y*-axis corresponds to the emissivity for *Grassland*.

Table 1
Analysis of emissivities under different subranges of viewing angles in bands 23 and 32.

Cover type	Band No.	Band 23		Band 32	
	Viewing angles	±(0°–45°)	±(45°–65°)	±(0°–45°)	±(45°–65°)
Grassland	Mean	0.917	0.922	0.967	0.964
	STDEV	0.002	0.003	0.001	0.001
	Max	0.921	0.927	0.969	0.968
	Min	0.915	0.918	0.966	0.962
	$\Delta(131)$[a]	0.012		0.007	
Cropland	Mean	0.953	0.957	0.972	0.970
	STDEV	0.001	0.002	0.001	0.001
	Max	0.955	0.960	0.973	0.972
	Min	0.952	0.954	0.971	0.967
	$\Delta(131)$	0.008		0.006	
Barren	Mean	0.883	0.889	0.969	0.967
	STDEV	0.002	0.007	0.0004	0.001
	Max	0.888	0.901	0.970	0.960
	Min	0.879	0.880	0.968	0.965
	$\Delta(131)$	0.022		0.01	

[a] $\Delta(131)$ is the difference of maximum and minimum emissivities under the whole 131 viewing angles.

separates the whole range of MODIS viewing zenith angles (55° was designed, but the actual value is 65° due to the Earth's curvature) into subranges and tries to select a pair of clear-sky daytime and nighttime MODIS observations at viewing angles in the same subranges whenever it is possible (Wan et al., 2004).

The current version of LST product is collection 5. Wang et al. (2007) and Wan (2008) examined the improvement of MODIS collection 5 LST&LSE products to deal with drawbacks in collection 4, such as pixels with cloud-contaminated LST values and those with missing valid LST values in areas under apparently clear-sky conditions. Three refinements from a total of eight are interesting for us: (1) the way of detecting clear-sky conditions by varying the confidence of the determination of clear-sky can increase the number of clear-sky pixels; (2) the number of subranges of viewing angels in the *day/night algorithm* is modified from 5 to 16; and (3) the grid size of retrieved LST&LSE is changed to 6 km × 6 km instead of 5 km × 5 km. The results in this paper were obtained using the spectral emissivity (bands 20–23, 29, 31, 32) of MODIS collection 4 LST&LSE products (MOD11B1) from the *day/night algorithm*, covering most of East Asia (Fig. 1) from 2000 to 2004. Although the first refinement increased the number of valid LST&LSE values in our study region, the huge number of valid values of 5-year collection 4 products in our study region is enough to make our result representative of this region. In terms of the second refinement, the accuracy of retrieved emissivity in collection 5 was enhanced, but the emissivity in collection 4 was also proved to be acceptable by validating the LST in clear-sky conditions (Wan et al., 2004, 2002). Therefore, application of collection 4 LST&LSE products is also reliable.

Another MODIS land product used in this paper was yearly land-cover product MOD12Q1, with a spatial resolution of 1 km. Both products (MOD11B1 and MOD12Q1) are distributed in 9 tiles covering most of East Asia (Fig. 1) from 2000 to 2004. This region covers various landscapes, including plateau, forest, irrigated crop, glacier, bare, and desert regions, and most of the study region was observed in large viewing angles; thus angular correction of LST is very much required.

2.2. Methods

Fig. 2 represents the flowchart of the data-picking method in this paper. Implementation of the method started with spatial aggregation of land cover products from 1 to 5 km. The new 5 km grid was considered as a "pure pixel or quasi-pure pixel" if no fewer than 23 1 km pixels of the total 5 × 5 1 km pixels are of the same cover type. Additionally, a cluster analysis was performed with the *eight-connectivity diagnosis* method to remove isolated pixels. Fig. 3 shows an example of cluster analysis on MODIS tile H26V04, located on the northeast corner of our study region (Fig. 1).

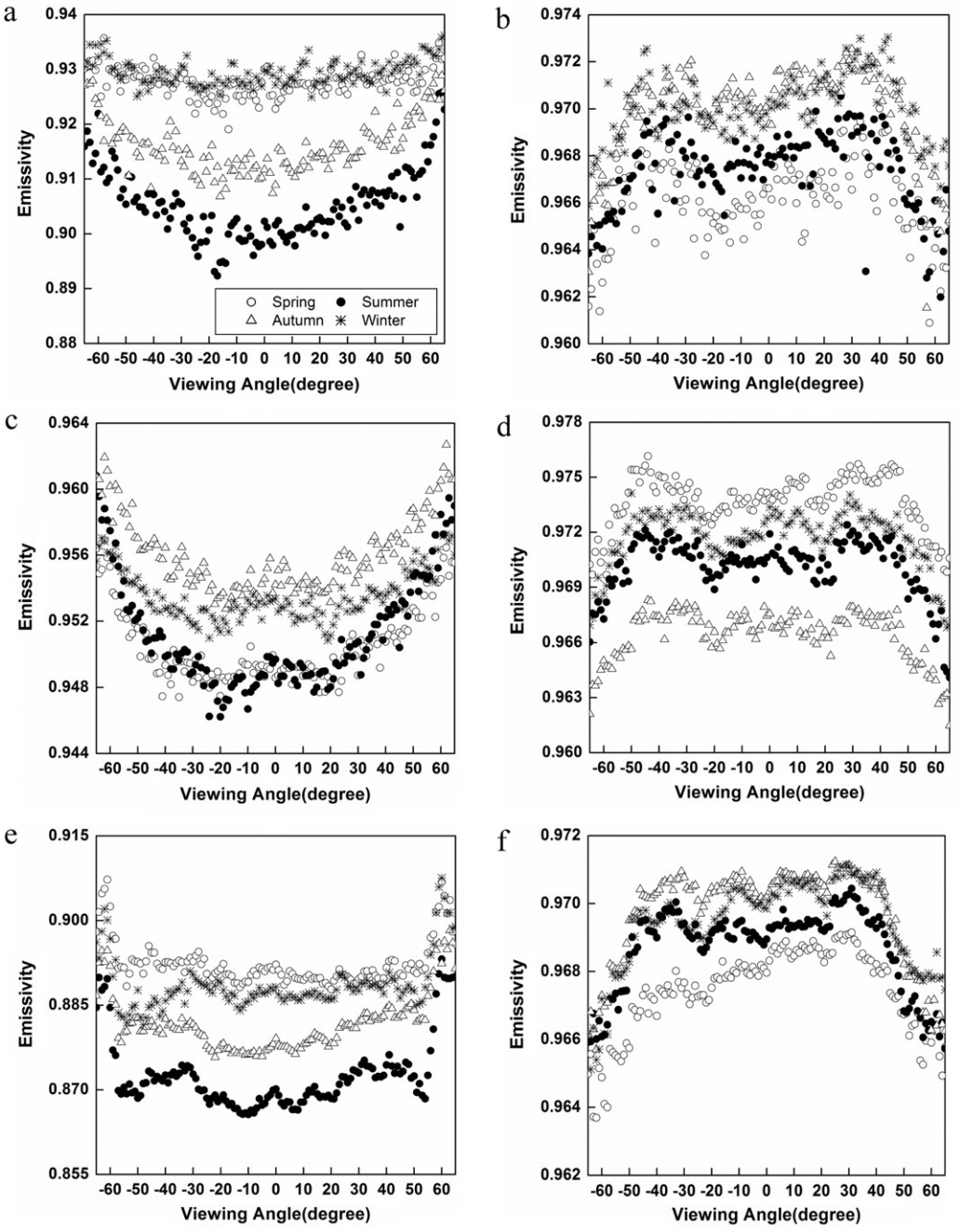

Fig. 6. Angular effects of emissivity in bands 23 and 32 in different seasons. (a), (c), and (e) show the emissivities in band 23 for *Grassland*, *Cropland*, and *Barren*, respectively; (b), (d), and (f) are those in band 32, respectively.

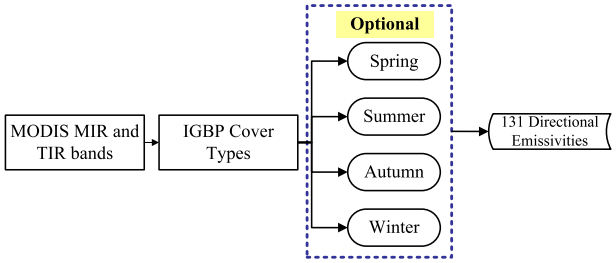

Fig. 7. The structures of look-up tables for directional emissivity. The optional frame means that the corresponding LUT is dependent on the seasons.

Besides the quality control flags, more constraints were used on the MODIS daily LST&LSE products to select the eligible pixels. First, the difference of viewing angles for a pixel between daytime and nighttime should be less than 4°, and then their average value was considered as the viewing angle of the pixel; second, the number of valid viewing angles for a specific cover type should be no less than 100 on a daily tile. The final selected pixels from the MODIS LST&LSE products were used to study the angular effects of emissivity.

3. Characteristics of MODIS emissivity

3.1. Angular effects of emissivity

After the data-picking step, directional emissivities for six cover types were obtained in our study region. They were *Grassland*,

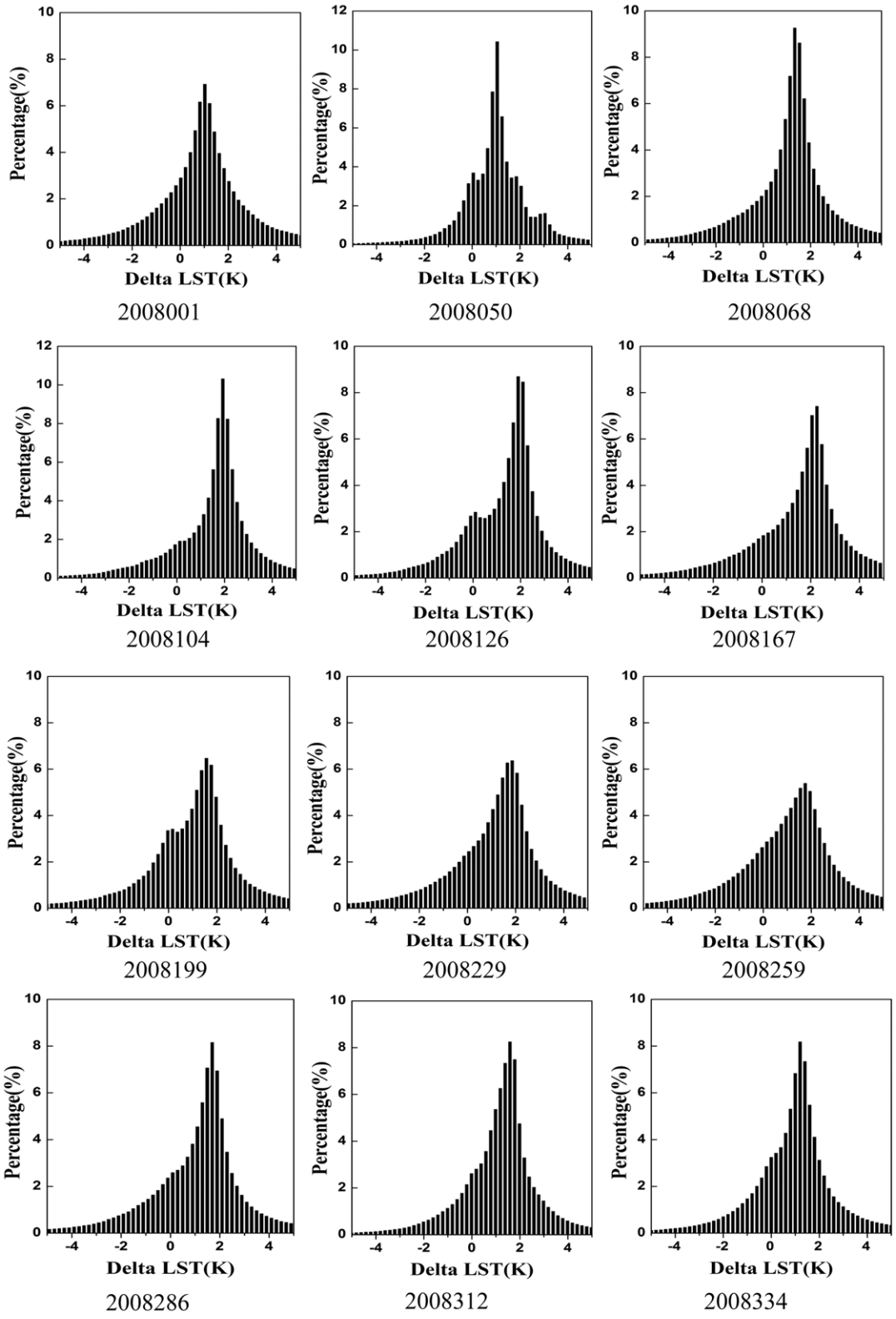

Fig. 8. Percentage histograms of temperature difference ΔT between newly retrieved LST and MODIS LST products of 12 scenes in 2008, located in the middle part of China.

Cropland, *Evergreen Broadleaf Forest*, *Mixed Forest*, *Open Shrublands* and *Barren or Sparsely Vegetated* (hereinafter abbreviated as *Barren*). Because of space limitations, we only take *Grassland*, *Cropland*, and *Barren* as examples to illustrate the angular effects of emissivity for the 5 km-scaled grid in six MODIS MIR and TIR bands mentioned above. Fig. 4(a), (c), and (e) show the directional emissivities in the MIR bands, and (b), (d) and, (f) show those in the TIR bands. It can be found that: (1) the emissivities increased with viewing angles in the MIR bands but decreased in the TIR bands; (2) they varied slightly from 0° to 45° but significantly when the viewing angles are larger than 45°; (3) the curves of directional emissivities in the MIR bands and TIR bands (except band 29 for *Barren*) showed similar shapes. Table 1 gives some statistical information about the directional emissivities of bands 23 and

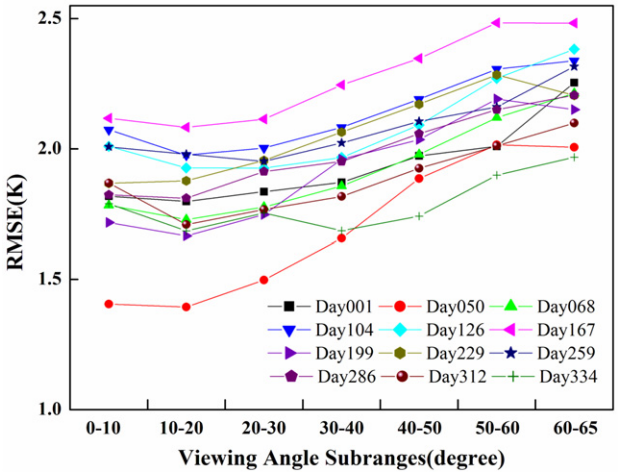

Fig. 9. RMSEs in seven viewing angle subranges.

32 for the three cover types. It can be found that the maximum differences in emissivities under all angles are about 0.01–0.02 in band 23 (which means an equivalent ΔT from 0.8 to 1.5 K at T = 300 K), and about 0.006 in band 32 (which means an equivalent ΔT about 0.5 K at T = 300 K). The directional emissivities of the other three cover types (*Evergreen Broadleaf Forest*, *Mixed Forest*, and *Open Shrublands*) presented similar tendencies in the MIR and TIR bands as *Grassland* and *Cropland* did.

Based on the above directional emissivities, we present the relationship between the emissivities and the cosine values of the viewing angles in bands 23 and 32 for *Grassland* and *Cropland* in Fig. 5(a) and (b). The curve of band 23 in Fig. 5(a) denotes a logarithmic relationship while Fig. 5(b) shows an exponential relationship. These relationships are simple and easy in use. Herein, Eq. (1) expresses the regressed results of *Cropland*'s emissivity versus the cosine of the viewing angle. Relationships for other cover types can be obtained similarly.

$$\begin{aligned}&\varepsilon(\theta) = -0.01\ln[\cos(\theta)] + 0.917, \quad R^2 = 0.91, \quad \text{for band 23}\\ &\varepsilon(\theta) = -0.0015\exp[-0.62\cos(\theta)] + 0.968,\\ &R^2 = 0.86, \quad \text{for band 32.}\end{aligned} \tag{1}$$

3.2. Angular effects in different seasons

As we know, emissivity is also influenced by the vegetation fraction. Vegetation fraction changes cannot be ignored during the year. Seasonal averaged directional emissivities were also obtained in this study. Fig. 6 presents the seasonal directional emissivities for *Grassland*, *Cropland* and *Barren* in bands 23 and 32. In general, the angular variation was similar in the four seasons. For band 23, the emissivities in summer and autumn were smaller than those in the other two seasons. The minimum emissivity value was found in summer, and the emissivity in summer was more sensitive to the change of viewing angle than that in other seasons. After changing the limitation of the minimum number of valid viewing angles on a daily tile from 100 to 85, we obtained the seasonal averaged directional emissivities of another four cover types (*Water, Woody Savannas, Urban and Built-up, and Permanent Snow and Ice*), and found the similar phenomena.

Based on the chosen directional emissivity, two look-up tables (LUTs) were created in this study. Both LUTs depend on the cover type and the viewing angle, but with the slight difference that one of them relies on the seasons (seasonal-dependent LUT). Their structures are described in Fig. 7. It should be noted that the emissivities in both LUTs were not calculated using Eq. (1) but were chosen directly from MODIS products at the 5 km scale. Both LUTs include the directional emissivities of *Grassland*, *Cropland*, *Evergreen Broadleaf Forest*, *Mixed Forest*, *Open Shrublands*, and *Barren or Sparsely Vegetated*. The seasonal-dependent LUT also includes the directional emissivities of another four cover types: *Water, Woody Savannas, Urban and Built-up, and Permanent Snow and Ice*. The emissivities of the remaining seven cover types in the IGBP scheme were also included in the seasonal-dependent LUT, but they were set to constant values according to Wan's paper (Wan, 2008).

4. Application to the split-window algorithm

4.1. The theory of the split-window algorithm

The *split-window algorithm* (Wan and Dozier, 1996; Wan et al., 2004) uses a linear combination of two apparent temperatures and the corresponding band-averaged emissivities to estimate the LST as follows:

$$\begin{aligned}T_s = C &+ \left(A_1 + A_2\frac{1-\varepsilon}{\varepsilon} + A_3\frac{\Delta\varepsilon}{\varepsilon^2}\right)\frac{T_{31}+T_{32}}{2}\\ &+ \left(B_1 + B_2\frac{1-\varepsilon}{\varepsilon} + B_3\frac{\Delta\varepsilon}{\varepsilon^2}\right)\frac{T_{31}-T_{32}}{2},\end{aligned} \tag{2}$$

where A_i, B_i (i = 1, 2, 3) and C are coefficients regressed from numerical simulation in MODTRAN code; T_{31} and T_{32} are the apparent temperatures of bands 31 and 32 of MODIS, respectively; $\varepsilon = 0.5(\varepsilon_{31} + \varepsilon_{32})$ and $\Delta\varepsilon = \varepsilon_{31} - \varepsilon_{32}$, where ε_{31} and ε_{32} are the classification-based emissivity (Snyder and Wan, 1998; Snyder et al., 1998). To account for the viewing angle effect, Wan et al. (2004) made a simple linear correction to the band emissivity when the viewing angle is larger than 45° for some land cover types, but this has not been used in the generation of MODIS LST products. The seasonal-dependent LUT was used in our framework to get the correction factor between the directional emissivities of MODIS bands 31 and 32, and angular dependence removed LSTs were obtained by using the correction factor in Eq. (2) at the 1 km scale. In the next section, the newly retrieved LST and the original MODIS 1 km LST products are compared.

4.2. Application and comparison

A total of 12 MODIS scenes (one per month in 2008) were chosen to calculate the angular dependence removed LST, most of them located in the middle and northwest part of China. The percentage histogram of temperature differences between the modified LST and MODIS 1 km LST products (MOD11_L2) are shown in Fig. 8. The figure indicates that the temperature difference (ΔT) for most pixels is in the range −1–3 K; the modified LSTs were generally greater than the MODIS LST products in most of cases. The peak ΔT values of the histograms varied from 1.02 to 2.26 K, and 9 of the 12 scenes show that the temperature differences were more than 1.5 K. Table 2 gives more information: about 45–55% of the pixels had temperature differences in the range peak $\Delta T \pm 1$ K, and 53–64% of the pixels had temperature differences in the range peak $\Delta T \pm 1.5$ K.

Further, we divided the viewing angles into seven subranges with an interval of 10°, and we present the root mean square errors (RMSEs) of the temperatures of the 12 scenes in Fig. 9. This figure shows that the RMSEs in all viewing angle subranges were within 1.4–2.5 K and the discrepancy between the maximum and minimum RMSEs was about 0.6 K. However, the RMSE increased with the increase of viewing angle. This is reasonable, because the modified LSTs tend to be larger at large viewing angles due to the lower emissivity values. From the above results, a conclusion can be drawn that the inversion of LST with a high accuracy is needed to consider the angular effects of emissivity, especially at large viewing angles.

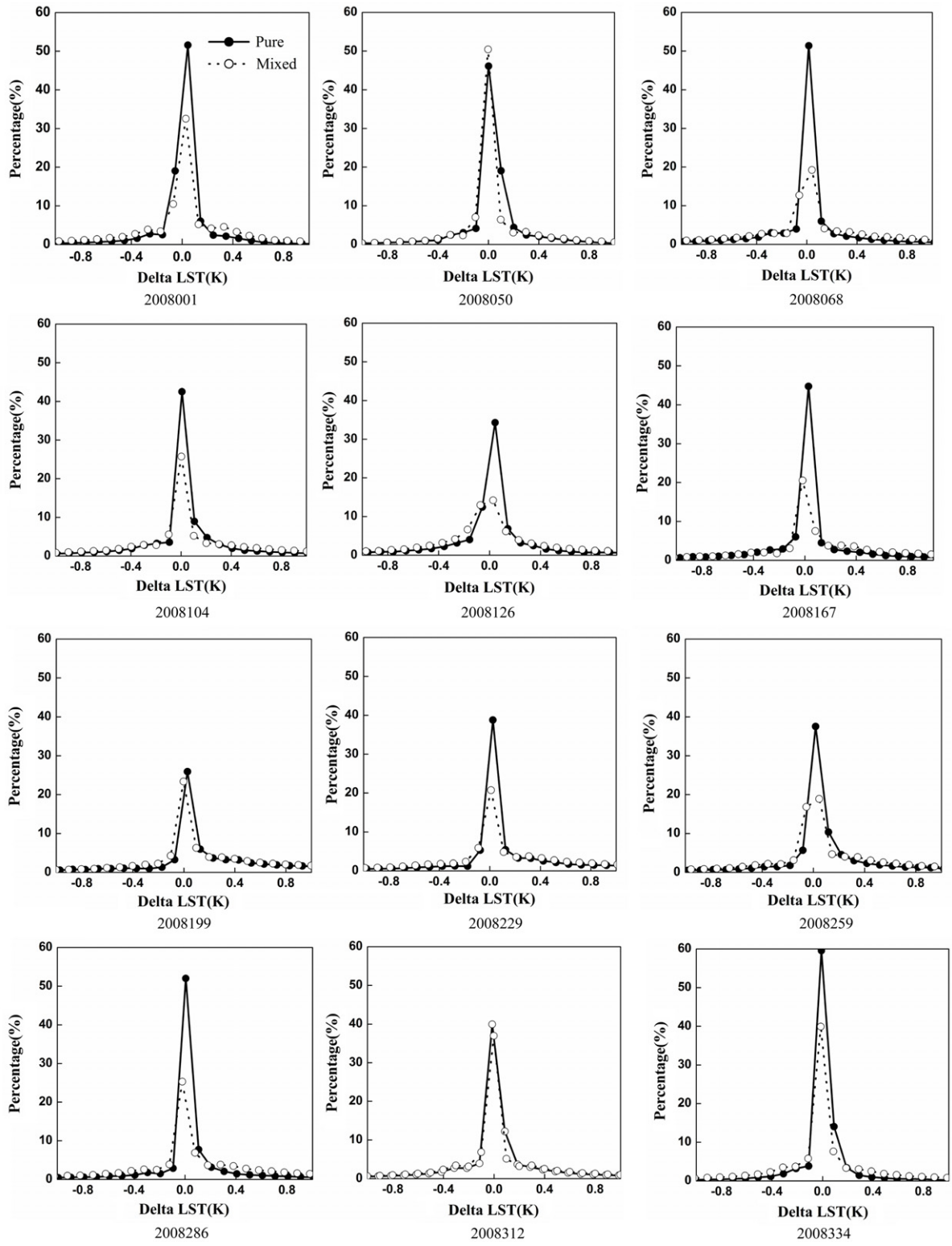

Fig. 10. Percentage histograms of ΔT_5 km data of 12 scenes for pure and mixed pixels at 5 km.

4.3. Spatial scale effects of emissivity

It is worth noticing that the emissivities in the LUTs were retrieved directly from the 5 km grid, which was assumed to be homogeneous. However, we have so far retrieved the LST at 1 km resolution. So, the spatial scale effects of emissivity that may influence the accuracy of LST should be considered. In order to check the scale effects, we retrieved the LST again at 5 km resolution with the same method and data applied previously. The 5 km brightness temperatures T_{31} and T_{32} in Eq. (2) were averaged from 5 × 5 1 km resolution pixels in MODIS L1B products, and pure or quasi-pure pixels and mixed pixels were distinguished using the same constraint shown in Fig. 2. Then the 5 km LST was retrieved (denoted as LST_5 km). By comparing with the 5 km LST (LST′_5 km) which was directly averaged from the 1 km modified LST mentioned before, the temperature difference

Table 2
Temperature differences in 12 scenes.

Day of 2008	Peak ΔT (K)	Percentages of pixels within the defined temperature differences (%)	
		Peak $\Delta T \pm 1$ K	Peak $\Delta T \pm 1.5$ K
1	1.02	46.4	57.9
50	1.04	50.9	62.5
68	1.33	53.8	63.7
104	1.93	54.6	64.3
126	1.90	50.7	60.5
167	2.26	45.4	55.7
199	1.57	45.0	56.2
229	1.86	45.6	56.8
259	1.75	41.5	53.2
286	1.69	49.1	59.3
312	1.59	51.7	62.7
334	1.20	50.8	62.3

caused by the scale effects can be expressed as $\Delta T\_5\ \text{km} = \text{LST}\_5\ \text{km} - \text{LST}'\_5\ \text{km}$. The percentage histograms of ΔT_5 km for pure and mixed pixels are presented in Fig. 10. The result shows that the percentage peaks of the temperature differences were very close to 0.0 K, and the differences fell within ±0.5 K for most pixels.

5. Conclusions and discussions

Using a statistical analysis of MODIS land cover products and LST&LSE products from the *day/night algorithm*, the angular effects of emissivity for several types of land cover in East Asia have been presented. The results show that the emissivities increased with the increase of viewing angle in MODIS MIR bands but decreased in TIR bands; and the angular effects caused the emissivity to vary by 0.01–0.02. Based on the directional emissivities, two LUTs at 5 km were created, and one of them was applied to the *split-window algorithm* to retrieve the LST at 1 km resolution. By comparing the retrieved LST with MODIS LST products, we found that new LSTs were generally larger than the MODIS LST products, and that the discrepancy ranged from −1 to +3 K. Large viewing angles can cause larger temperature differences than smaller ones. Finally, we discussed the spatial scale effects between the LST retrieval results at 1 and 5 km; the corresponding result showed that the spatial scale effects of emissivity could be ignored from 1 to 5 km in our study region.

The relationship between fractional vegetation cover and emissivity has been discussed in detail (Momeni and Saradjian, 2007, Sobrino et al., 2001 and Sobrino et al., 2008). However, the angular effect of emissivity itself was seldom considered in the past. Seasonal directional emissivities haven been obtained in this paper. Following this framework, further research may be done by considering the fractional vegetation cover and angular effects together in the modeling of emissivity.

Besides, our study on emissivity was performed only over most of East Asia, and not all the land cover types in the IGBP scheme and global coverage were included in our result. Therefore, future work can be extended to more regions and land cover types. Currently, the modified LST after correcting the angular dependence was compared only with the original MODIS LST products. If ground-based reliable measurements over sufficiently large areas are available in the future, the temperature validation work will be done in forthcoming studies. By our field experiences, new data collection methods and effective equipment are needed to get more reliable in situ LST values.

Acknowledgements

The authors would like to thank Professor Zhengming Wan for his explanations of the *split-window algorithm* and the *day/night algorithm* in detail. We thank Mr. Brett from NASA Land Processes Distributed Active Archive Center User Services and his colleagues for their help on the understanding of EOS HDF format and the downloading of MODIS products. We would also like to thank the anonymous reviewers for their valuable suggestions and comments.

References

Barton, I.J., Talashima, T., 1986. An AVHRR investigation of surface emissivity near Lake Eyre, Australia. Remote Sensing of Environment 20 (2), 153–163.
Becker, F., Li, Z., 1990a. Temperature-independent spectral indices in thermal infrared bands. Remote Sensing of Environment 32 (1), 17–33.
Becker, F., Li, Z., 1990b. Towards a local split window method over land surface. International Journal of Remote Sensing 11 (3), 369–393.
Borel, C.C., 1998. Surface emissivity and temperature retrieval for a hyperspectral sensor. In: IEEE International, Geoscience and Remote Sensing Symposium Proceedings, 6–10 July, pp. 546–549.
Caselles, V., Sobrino, J.A., 1992. A physical model for interpreting the land surface temperature obtained by remote sensors over incomplete canopies. Remote Sensing of Environment 39 (3), 203–211.
Chen, L., Zhuang, J., Xu, X., Liu, Q., 2000. Measurement of directional emissivity in lab using two-channel and two-temperature method. Journal of Remote Sensing 4 (Suppl.), 64–70.
Duan, S., Yan, G., Qian, Y., Li, Z., Jiang, X., Li, X., 2008. Retrieval of land surface temperature from simulated HJ-1B data using two different single channel methods. Progress in Natural Science 18 (9), 1001–1008.
Enric, V., Vicente, C., 1996. Mapping land surface emissivity from NDVI: application to European, African, and south American areas. Remote Sensing of Environment 19 (14), 2753–2774.
François, C., Ottlé, C., Prévot, L., 1997. Analytical parameterization of canopy directional emissivity and directional radiance in the thermal infrared. Application on the retrieval of soil and foliage temperatures using two directional measurements. International Journal of Remote Sensing 18 (12), 2587–2621.
Gillespie, A., Rokugawa, S., Matsuuaga, T., Hook, S., Kahle, A., 1998. A temperature and emissivity separation algorithm for advanced spaceborne thermal emission and reflection radiometer (ASTER) images. IEEE Transactions on Geoscience and Remote Sensing 36 (4), 1113–1126.
Ingram, P.M., Muse, A.H., 2001. Sensitivity of iterative spectrally smooth temperature/emissivity separation to algorithmic assumptions and measurement noise. IEEE Transactions on Geoscience and Remote Sensing 39 (10), 2158–2257.
Jiménez-Muñoz , Sobrino J.A., 2003. A generalized single-channel method for retrieving land surface temperature from remote sensing data. Journal of Geophysical Research 108 (D22), 4688. doi:10.1029/2003JD003480.
Kahle, A.B., Madura, D.P., Soha, J.M., 1980. Middle infrared multispectral aircraft scanner data: analysis for geological applications. Applied Optics 19 (14), 2279–2290.
Kealy, P.S., Hook, S.J., 1993. Separating temperature and emissivity in thermal infrared multispectral scanner data: implications for recovering land surface temperatures. IEEE Transactions on Geoscience and Remote Sensing 31 (6), 1155–1164.
Kimes, D.S., Kirchener, J.A., 1983. Directional radiometric measurements of row-crop temperatures. International Journal of Remote Sensing 4 (2), 299–311.
Labed, J., Stoll, M.P., 1991. Spatial variability of land surface emissivity in the thermal infrared band: spectral signature and effective surface temperature. Remote Sensing of Environment 38 (1), 1–17.
Lagouarde, J.P., Kerr, Y.H., Brunnet, Y., 1995. An experimental study of angular effects on surface temperature for various plant canopies and bare soils. Agricultural and Forest Meteorology 77 (3–4), 167–190.
Li, X., Strahler, A.H., 1992. Geometric–optical bidirectional reflectance modeling of the discrete crown vegetation canopy: effect of crown shape and mutual shadowing. IEEE Transactions on Geoscience and Remote Sensing 30 (2), 276–292.
Li, X., Strahler, A.H., Fried, M.A., 1999. A conceptual model for effective directional emissivity from nonisothermal surfaces. IEEE Transactions on Geoscience and Remote Sensing 37 (5), 2508–2517.
Liu, Q., Chen, L., Liu, Q., Xiao, Q., 2003. A radiation transfer model to predict canopy radiation in thermal infrared band. Journal of Remote Sensing 7 (3), 161–167.
Mannstein, H., 1987. Surface energy budget, surface temperature, and thermal inertia. In: R.A. Vaughan and D. Reidel, (Eds.), Remote Sensing Applications in Meteorology and Climatology, Netherlands, Dordrecht.
McMillin, L.M., 1975. Estimation of sea surface temperature from two infrared window measurements with different absorption. Journal of Geophysical Research 80 (C36), 5113–5117.
Momeni, M., Saradjian, M.R., 2007. Evaluating NDVI-based emissivities of MODIS bands 31 and 32 using emissivities derived by Day/Night LST algorithm. Remote Sensing of Environment 106 (2), 190–198.

Petitcolin, F., Nerry, F., Stoll, M.-P., 2002a. Mapping directional emissivity at 3.7 um using a simple model of bi-directional reflectivity. International Journal of Remote Sensing 23 (17), 3443–3472.
Petitcolin, F., Nerry, F., Stoll, M.-P., 2002b. Mapping temperature independent spectral indices of emissivity and directional emissivity in AVHRR channels 4 and 5. International Journal of Remote Sensing 23 (17), 3473–3491.
Prata, A.J., 1993. Land surface temperatures derived from the AVHRR and ATSR 1, theory. Journal of Geophysical Research 89 (16), 689–702.
Price, J.C., 1983. Estimating surface temperature from satellite thermal infrared data–a simple formulation for the atmospheric effect. Remote Sensing of Environment 13 (4), 353–361.
Qin, Z., Zhang, M., Karnieli, A., Berliner, P., 2001. Mono-window algorithm for retrieving land surface temperature from Landsat TM6 data. Journal of Remote Sensing 56 (4), 456–466.
Snyder, W.C., Wan, Z., 1998. BRDF models to predict spectral reflectance and emissivity in the thermal infrared. IEEE Transactions on Geoscience and Remote Sensing 36 (1), 214–225.
Snyder, W.C., Wan, Z., Feng, Y.-Z., 1998. Classification-based emissivity for land surface temperature measurement from space. International Journal of Remote Sensing 9 (14), 2753–2774.
Sobrino, J.A., Caselles, V., 1990. Thermal infrared radiance model for interpreting the directional radiometric temperature of a vegetative surface. Remote Sensing of Environment 33 (3), 193–199.
Sobrino, J.A., Jiménez-Muñoz, J.C., Sòria, G., Romaguera, M., Guanter, L., 2008. Land surface emissivity retrieval from different VNIR and TIR sensors. IEEE Transactions on Geoscience and Remote Sensing 46 (2), 316–327.
Sobrino, J.A., Jiménez-Muñoz, J.C., Verhoef, W., Bendikov, T.A., 2005. Canopy directional emissivity: comparison between models. Remote Sensing of Environment 99 (3), 304–314.
Sobrino, J.A., Raissouni, N., Li, Z., 2001. A comparative study of land surface emissivity retrieval from NOAA data. Remote Sensing of Environment 75 (2), 256–266.
Su, Z., 2002. The surface energy balance system (SEBS) for estimation of turbulent heat fluxes. Hydrology and Earth System Sciences 16 (1), 85–99.
Su, L., Li, X., Wang, J., 2000b. Simulation of thermal exitance from homogeneous canopy. Journal of Remote Sensing 4 (Suppl.), 53–58.
Su, L., Li, X., Wang, J., Liu, Q., 2000c. Field experiment validation for the LSF conceptual model on directional thermal emissivity of non-isothermal surfaces. Journal of Remote Sensing 4 (Suppl.), 81–85.
Su, H., Wang, J., Li, X., Zhang, R., Tang, X., Sun, X., 2000a. The indoor simulation and validation of thermal radiation directionality model for three dimensional surfaces with heterogeneous temperature. Journal of Remote Sensing 4 (Suppl.), 71–80.
Van, d.G., Owe, M., 1993. On the relationship between thermal emissivity and the normalized difference vegetation index for natural surfaces. International Journal of Remote Sensing 14 (6), 1119–1131.
Verhoef, W., Jia, L., Xiao, Q., Su, Z., 2007. Unified optical–thermal four-stream radiative transfer theory for homogeneous vegetation canopies. IEEE Transactions on Geoscience and Remote Sensing 45 (6), 1808–1822.
Wan, Z., 2008. New refinements and validation of the MODIS land-surface temperature/emissivity products. Remote Sensing of Environment 112 (1), 59–74.
Wan, Z., Dozier, J., 1996. A generalized split-window algorithm for retrieving land-surface temperature from space. IEEE Transactions on Geoscience and Remote Sensing 34 (4), 892–905.
Wan, Z., Li, Z., 1997. A physics-based algorithm for retrieving land-surface emissivity and temperature from EOS/MODIS data. IEEE Transactions on Geoscience and Remote Sensing 35 (4), 980–996.
Wan, Z., Zhang, Y., Zhang, Q., Li, Z., 2002. Validation of the land-surface temperature products retrieved from terra moderate resolution imaging spectroradiometer data. Remote Sensing of Environment 83 (1–2), 163–180.
Wan, Z., Zhang, Y., Zhang, Q., Li, Z.-L., 2004. Quality assessment and validation of the MODIS global land surface temperature. International Journal of Remote Sensing 25 (1), 261–274.
Wang, K., Wan, Z., Wang, P., Sparrow, M., Liu, J., Haginoya, S., 2007. Evaluation and improvement of the MODIS land surface temperature/emissivity products using ground-based measurements at a semi-desert site on the western Tibetan Plateau. International Journal of Remote Sensing 28 (11), 2549–2565.
Watson, K., 1992. Spectral ratio method for measuring emissivity. Remote Sensing of Environment 42 (2), 113–116.
Zhao, Y., 2003. Theories and Methodology for the Application of Remote Sensing. Science Press, Beijing, China.